Chinese Chemical Letters 36 (2025) 109959

Contents lists available at ScienceDirect

Chinese Chemical Letters

journal homepage: www.elsevier.com/locate/cclet

Enrichment-enhanced detection strategy in the optimized monitoring system of dopamine with carbon dots-based probe

Xilin Bai, Wei Deng, Jingjuan Wang*, Ming Zhou*

Key Laboratory of Polyoxometalate and Reticular Material Chemistry of Ministry of Education, National and Local United Engineering Laboratory for Power Batteries, Key Laboratory of Nanobiosensing and Nanobioanalysis at Universities of Jilin Province, Department of Chemistry, Analysis and Testing Center, Northeast Normal University, Changchun 130024, China

ARTICLE INFO

Article history:
Received 14 December 2023
Revised 28 March 2024
Accepted 30 April 2024
Available online 1 May 2024

Keywords:
Enrichment-enhanced detection strategy
Optimizing pathway
Improved sensitivity
Dopamine
Visual detection

ABSTRACT

The complexity of living environment system demands higher requirements for the sensitivity and selectivity of the probe. Therefore, it is of great importance to develop a universal strategy for high-performance probe optimization. Herein, we propose a novel "Enrichment-enhanced Detection" strategy and use carbon dots-dopamine detection system as a representative model to evaluate its feasibility. The composite probe carbon dots (CDs)-encapsulated in glycol-chitosan (GC) (*i.e.*, CDs@GC) was obtained by simply mixing GC and CDs through noncovalent interactions, including electrostatic interactions and hydrogen bonding. Dopamine (DA) could be detected through internal filter effect (IFE)-induced quenching of CDs. In the case of CDs@GC, noncovalent interactions (electrostatic interactions) between GC and the formed quinone (oxide of DA) could selectively extract and enrich the local concentration of DA, thus effectively improving the sensitivity and selectivity of the sensing system. The nanosensor had a low detection limit of 3.7 nmol/L, which was a 12-fold sensitivity improvement compared to the bare CDs probes with similar fluorescent profiles, proving the feasibility of the "Enrichment-enhanced Detection" strategy. Further, to examine this theory in real case, we designed a highly portable sensing platform to realize visual determination of DA. Overall, our work introduces a new strategy for accurately detecting DA and provides valuable insights for the universal design and optimization of superior nanoprobes.

Design of high-performance probes with enhanced sensitivity is crucial in detecting biomarkers for the early diagnosis of degenerative diseases [1–3]. Based on the unique structural and functional advantages of nanomaterials [4–6], several meticulously designed probes have been proven effective in various sensing scenarios [7–10]. However, many of these probes necessitate sophisticated fabrication techniques and have high manufacturing costs. Therefore, there is still a significant demand for universal strategies that can easily and systematically upgrade conventional probes to meet the requirements of cutting-edge, high-demanding detections.

Previously, we successfully developed a unique fluorescence platform by incorporating gold nanoclusters (AuNCs) into a nanogel of chitosan derivative, glycol chitosan (GC) [11]. This GC assembly served a dual purpose: it not only confined the Au clusters to enhance the fluorescent intensity of the probe but also utilized the positively charged amino groups of GC to attract sulfide ions through electrostatic forces, thereby synergistically improving the sensitivity of the detection. However, the preliminary idea of Enrichment-enhanced Detection Strategy was yet to be verified independently.

Dopamine (DA) is a crucial neurotransmitter and chemical messenger in central and peripheral nervous systems, which plays key roles in human metabolism, immune, memory and cognition [12–15]. The DA fluctuation is closely connected to severe physical and neurological diseases including Alzheimer, Parkinson, schizophrenia [16–18]. The diagnosis of these diseases requires high-precision measurement of DA. Various techniques have been developed for the sensitive detection of DA. Among them, fluorescent sensing is considered as one of the most promising detection strategies owing to its high sensitivity, good selectivity and real-time merits [19–22]. Carbon dots (CDs), as a new type of carbon-based material, have gained significant attention in recent years due to their unique optical properties, low cytotoxicity, and easy fabrication process [23,24]. Their potential applications range from bioimaging to biosensing [25]. For example, Soto *et al.* reported a N-doped carbon dots for highly sensitive and selective detection of DA in human fluids at nanomolar concentrations [26]. In another study, Liang *et al.* developed a carbon dots-gold nanoclusters hybrid for

* Corresponding authors.
E-mail addresses: wangjj863@nenu.edu.cn (J. Wang), zhoum739@nenu.edu.cn (M. Zhou).

https://doi.org/10.1016/j.cclet.2024.109959
1001-8417/

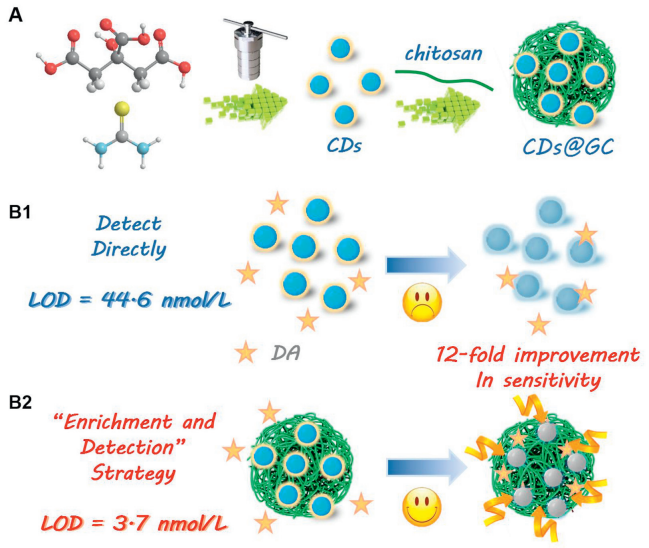

Scheme 1. Schematic of the synthesis of probe (A) and the sensing mechanism of CDs (B1), CDs@GC (B2).

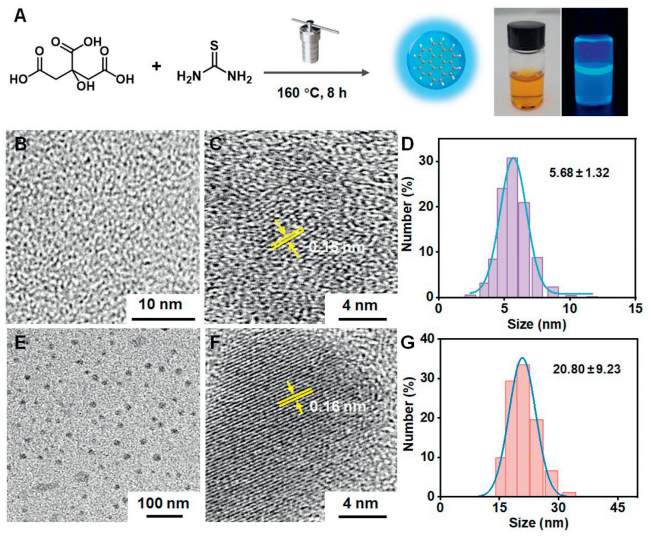

Fig. 1. (A) The synthesis route of CDs and its photograph under daylight and UV lamp (365 nm) illumination. TEM and HRTEM images of CDs (B, C) and CDs@GC (E, F). Size distribution of CDs (D) and CDs@GC (G).

the ratiometric fluorescence detection of DA [27]. Li *et al.* fabricated a series of graphene quantum dots to explore the influence of element doping on fluorescence sensing of DA [28]. However, in the case of DA-sensing, the complicated analytical environment, extremely low DA level still recalls for more smart and effective strategies to systemically upgrade the probes for DA sensing.

In this study, we used the CDs encapsulated in DA (CDs@GC) detection system as a representative model to rule-out the enhancement of fluorescent intensity and validate the feasibility of the Enrichment-enhanced Detection strategy (EED strategy) independently. As shown in Scheme 1, the CDs were prepared by one-step hydrothermal method. By mixing the CDs with GC, the self-assembled CDs@GC probe was easily obtained through noncovalent interactions such as electrostatic interactions and hydrogen bonding. Studies have shown that DA could form DA quinone by ambient O_2 in alkaline condition [29,30], and quenched the fluorescence of nanoprobes. The positively charged amino groups on the surface of GC could enable noncovalent interaction with DA-DA quinone through electrostatic interactions. Despite having nearly identical fluorescent profiles, the assembled CDs@GC probe exhibited a 12-fold increase in sensitivity compared to the bare CDs probes, thus confirming the feasibility of the EED strategy. We believe that this EED strategy presents a promising approach to optimizing conventional probes in high-demand detection scenarios.

In a typical procedure, CDs were synthesized *via* the hydrothermal technique using citric acid and thiourea as precursors (Fig. 1A). The obtained brownish solution exhibited good aqueous solubility and showed strong fluorescence under UV irradiation. The CDs@GC were easily obtained *via* noncovalent interactions including electrostatic interaction and hydrogen bond. The purified CDs and CDs@GC were characterized using various techniques to determine their structural and morphological composition. Fig. 1B shows the transmission electron microscopy (TEM) images of the CDs and exhibited a uniform dispersion without apparent aggregation. The high-resolution TEM images of CDs showed a lattice spacing of 0.15 nm, which is close to the (100) facet of graphite carbon (Fig. 1C). Dynamic light scattering (DLS) analysis were also conducted and the average particle size of CDs were about 6 nm (Fig. 1D). After assembled with GC, a well-organized self-assembled structure were obtained (Figs. 1E and F) and the average size of CDs@GC was increased to about 21 nm (Fig. 1G). Moreover, Fourier transform infrared (FTIR) and X-ray photoelectron spectroscopy (XPS) experiments were conducted to investigate the functional groups of the CDs@GC. In the FTIR analysis, the stretching vibrations of O-H, N-H, C-H, and C=O were clearly observed (Fig. S1 in Supporting information). Further, Fig. S2A (Supporting information) shows that the CDs@GC comprised carbon, nitrogen, oxygen, and sulfur. In Fig. S2B (Supporting information), the spectrum of N 1s demonstrates the presence of pyridinic N at 399.5 eV, pyrollic N at 400.0 eV, and graphitic N at 401.5 eV. The high-resolution spectrum of C 1s (Fig. S2C in Supporting information) reveals peaks at 284.4 eV, 285.0 eV and 287.4 eV, which are corresponded to the C=C/C–C, C-N and N-C=O bonds. The O 1s XPS spectrum in Fig. S2D (Supporting information) shows two peaks at 531.1 eV and 532.6 eV, which are attributed to C–OH and C=O. Excitation-dependent PL behavior of CDs and CDs@GC were investigated, which is common in fluorescent carbon materials due to the complex surface state affecting the band gap of CDs (Fig. S3A and S3B). Both of CDs and CDs@GC displayed satisfied quantum yield (QY) of 21.7% and 23.5% (using quinine sulfate as a reference, Fig. S4 and Table S1 in Supporting information).

Furthermore, the PL stability of CDs and CDs@GC to the effects of pH and ionic strength were investigated. According to Figs. S3C and D (Supporting information), the PL intensity remained stable when the pH adjusted from 6 to 12. Meanwhile, there was negligible influence on the fluorescence intensity of CDs or CDs@GC even the salinity was up to 3 mol/L (Figs. S3E and F in Supporting information). In addition, the stability of the as-prepared CDs and CDs@GC was evaluated (Fig. S5 in Supporting information). The fluorescence of CDs and CDs@GC remained almost unchanged after 4 h of continuous irradiation under UV light, which reveals the ideal photostability of the probes. Besides, only about 5% fluorescence decreased at the end of 8-week period when stored at 4 °C, indicating the satisfactory long-term stability of both CDs and CDs@GC. These indicated that CDs and CDs@GC exhibited almost identical fluorescent profiles including excitation-dependent PL behavior and PL stability in despite of the difference in morphology.

Before performing the sensitivity assay, detection parameters (pH, temperature and incubation time) were optimized for the system. As shown in Fig. S6A (Supporting information), the value of $\Delta I/I_0$ increased within the pH range from 6.0 to 11.0. It has been reported that DA could produce polydopamine in strong alkaline solutions, which is not conducive to sensitive detection of

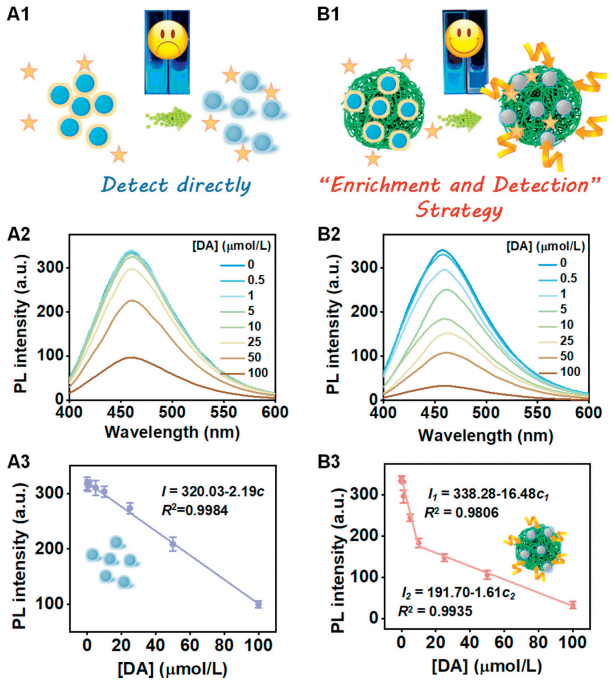

Fig. 2. Scheme illustration of fluorescence detection of DA by CDs (A1) and CDs@GC (B1). Fluorescence spectra of CDs (A2) and CDs@GC (B2) treated with various concentrations of DA; Calibration plot of the PL intensity *versus* the concentration of DA for CDs (A3) and CDs@GC (B3), respectively.

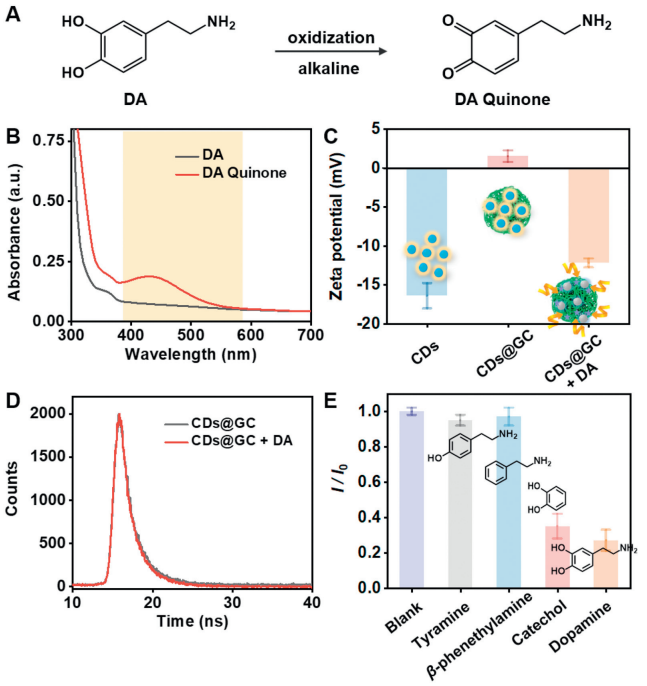

Fig. 3. (A) Schematic illustrating the DA oxidation process. (B) UV–vis absorption spectra of DA (black line) and DA Quinone (red line). (C) Zeta potential of the system. (D) PL lifetime measurement of CDs@GC in the absence and presence of DA. (E) Effect of the DA homologues on the fluorescence quenching performance of CDs@GC.

dopamine. Therefore, moderate alkali condition (pH 9.0) was selected for the sensing system. On the other hand, temperature affects the reaction rate, which is of great significance to the detection process. As shown in Fig. S6B (Supporting information), 50 °C is the optical reaction temperature. The incubation time of the reaction system was also investigated to determine the optimal response time of the fluorescence sensor. According to Fig. S6, the value of $\Delta I/I_0$ increased dramatically within 1 h; while after 1 h, slight increases could be observed. To achieve a satisfied response, 1 h of pre-incubation time was used for further experiments.

Under optical conditions, PL spectra of CDs@GC as well as bare CDs with 0.5–100 μmol/L DA was studied and showed in Fig. 2. The PL intensity of CDs and CDs@GC at 460 nm gradually decreased with the increase of DA concentrations (Figs. 2A2 and B2), and was quenched along with the increasing concentration of DA. For CDs, the linear equation is calculated $I = 320.03 - 2.19c$ with a correlation coefficient of 0.9984 (Fig. 2A3). While for CDs@GC, the linear regression equation is $I_1 = 338.28 - 16.48c_1$ for low concentration (≤10 μmol/L) and $I_2 = 191.70 - 1.61c_2$ for higher concentration (≥10 μmol/L), with a correlation coefficient of 0.9806 and 0.9935, respectively (Fig. 2B3). The limit of detection ($LOD = 3\sigma/K$) for DA was 44.6 nmol/L for CDs and 3.7 nmol/L for CDs@GC. Impressively, though with similar fluorescent property, the CDs@GC achieved 12-fold improvement in the sensitivity than the bare CDs. Thus, it was the change of interaction between probe and DA rather than the change of fluorescent profile that contribute to the enhancement of DA sensing.

The dependence of the intensity of luminescence with increasing concentrations of DA followed the Stern-Volmer formalism: $I_0/I = 1 + K_{SV}[DA]$, where I_0 is the luminescence signal of CDs in the absence of DA, and I is the luminescence signal with an increasing concentration of DA. K_{SV} is the Stern-Volmer constant, which indicates the quenching efficiency between the nanoprobes and DA. The calculated K_{SV} were found to be 0.00909 and 0.08632 for CDs and CDs@GC, respectively, which confirmed the assembled GC indeed promoted sensitive detection of DA.

The selectivity of the probes toward DA were also studied. Under identical conditions, only DA displayed a significant luminescence quenching, while other species (Na^+, K^+, Ca^{2+}, Mg^{2+}, GSH, Ala, Gly, Phe, Leu, glucose, tyramine, β-phenethylamine and catechol) produced negligible fluorescence changes even at the concentration of 10-fold higher than that of DA (Fig. S7 in Supporting information). Comparing with some other fluorescent nanoprobes, CDs@GC also has excellent sensitivity (Table S2 in Supporting information).

Dopamine could be easily oxidized to quinone by ambient O_2 in alkaline conditions (Fig. 3A) [29,30]. Herein, to investigate the sensing mechanism, the UV–vis absorption spectra of DA and DA quinone have been measured. As shown in Fig. 3B, the emission spectrum of CDs@GC (yellow region) shows obvious spectral overlap with the absorption band of generated DA quinone, which directly cause the fluorescence quenching of the probe. The zeta potential of the sensing system was also detected. As shown in Fig. 3C, the CDs are negatively charged and the zeta potential is about -16.43 mV. Whereas the CDs@GC are positively charged with a zeta potential of 2.56 mV, suggesting the nanocomplex has been successfully formed. When adding 50 μmol/L DA to the solution, the zeta potential of CDs@GC decreased to -12.21 mV. The anion-cation pair of DA^- and CDs@GC-NH_2^+ could be formed *via* electrostatic interaction, which makes DA possess a special affinity to the CDs@GC. Meanwhile, studies have demonstrated that quinones could dynamically react with chitosan's amines *via* Michael addition or Schiff base reaction [31-33] and form a DA "reservoir" to further raise the regional DA concentration. Thus, the DA could be electrostatically attracted and dynamically bonded to the CDs@GC probe, which could synergistically contribute to the good sensitivity and selectivity.

Complexes formation induced fluorescence quenching is general categorized to static quenching. Herein, the time-resolved fluorescence spectra of the CDs@GC with/without DA were measured to verify the quenching mechanism. The fluorescence decay curves

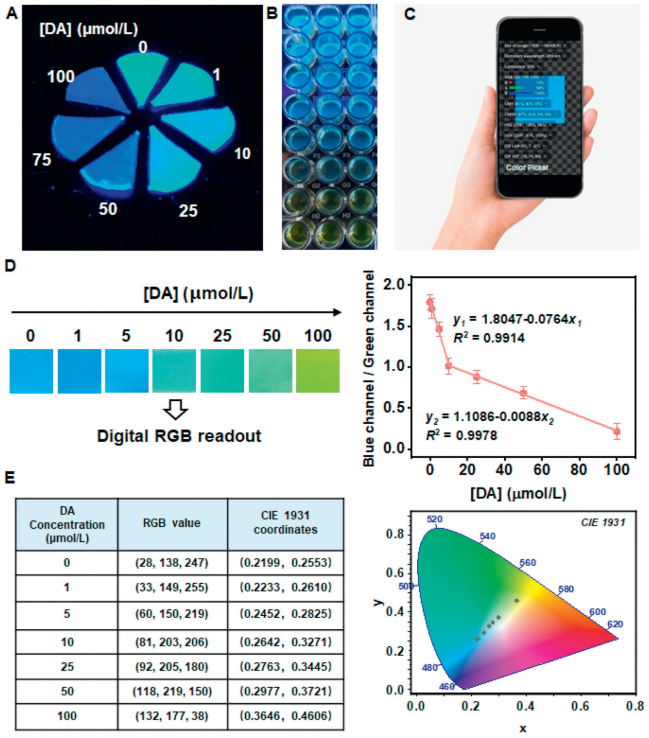

DA Concentration (μmol/L)	RGB value	CIE 1931 coordinates
0	(28, 138, 247)	(0.2199, 0.2553)
1	(33, 149, 255)	(0.2233, 0.2610)
5	(60, 150, 219)	(0.2452, 0.2825)
10	(81, 203, 206)	(0.2642, 0.3271)
25	(92, 205, 180)	(0.2763, 0.3445)
50	(118, 219, 150)	(0.2977, 0.3721)
100	(132, 177, 38)	(0.3646, 0.4606)

Fig. 4. (A) The visual detection of DA on filter paper. (B) The visual detection of DA after addition of riboflavin into the system. (C) Photos taken and displayed through the Color Picker APP. (D) FL evolution images with the addition of DA captured *via* a smartphone and linear fitting curve of B/G against the concentration of DA. (E) Relative RGB value and CIE value graph corresponding to different DA concentrations.

are shown in Fig. 3D. In the absence and presence of DA, the fluorescence lifetimes of the CDs@GC were almost the same, implying that the quenching mechanism obeys static quenching rather than dynamic quenching. The overlap between absorbance spectrum of the acceptor (DA quinone species) and excitation spectrum of the donor (CDs@GC), and the constant lifetime value demonstrated the occurrence of inner filter effect (IFE) process in the system. Furthermore, three DA homologues (tyramine, β-phenethylamine and catechol) were chosen to explore the fluorescence quenching behavior of CDs@GC. As shown in Fig. 3E, both tyramine and β-phenethylamine hardly show any fluorescence quenching phenomenon, while the catechol and DA both exhibit fluorescence quenching to some extent. Therefore, we deduce that the catechol group is the crucial structure for the quenching of CDs@GC, which is consistent with the above results.

In recent years, the portability and practicality of smartphones have been favored in various detection fields [34-36]. The related applications on smartphones can transform color signals into digital dataset for analysis to achieve the quantitative detection of analytes. To verify the possibility of the sensing platform, firstly we tested the sensing system on filter paper. As shown in Fig. 4A, with the concentration of DA increases, the fluorescence intensity of the filter paper significantly decreased. Considering that single color change (dark blue to light blue) could not be easily recognized, we added a common fluorescent dye, riboflavin into the system. With the increase of DA concentration, the fluorescence of the system showed a change from blue to yellow, demonstrating the feasibility for the construction of the sensing platform (Fig. 4B). Next, the portable sensing platform was created by the combination of a smartphone, a mini laser, a sample curve and a dark chamber. The RGB values corresponding to the photos are obtained through a color recognizer APP (Color Picker) for further statistical analysis (Fig. 4C). After the reaction was completed, a series of photos with colors ranging from blue to yellow green were taken with a smartphone under a 365 nm ultraviolet mini-laser. According to Fig. 4D, there is a good linear relationship between the RGB ratio (B/G) and the DA concentration. The low concentration linear regression equation is $y_1 = 1.8047 - 0.0764x_1$ and high concentration linear regression equation is $y_2 = 1.1086 - 0.0088x_2$, with a correlation coefficient of 0.9914 and 0.9978, respectively. In addition, the corresponding CIE chromaticity coordinates shift from the blue area to the yellow area, thus realizing the visual determination of DA (Fig. 4E). The above results indicate that the probe has a more sensitive response in the low concentration range. More importantly, compared with the standard curve measured in solution state, the ratio of the slopes of the two segments is almost equal, indicating the reliability of digital signal conversion for dopamine detection (Table S3 in Supporting information).

To test the practicability of the CDs@GC nanosensor, the concentration of DA in human sweat samples and urine samples was detected using standard addition method, and the results are shown in Tables S4 and S5 (Supporting information). Under optimized conditions, the mean recoveries of the spiked samples were in the range of 90%–115% with the relatively low relative standard deviation (RSD) under 1.0% at spiked concentrations of 10, 15, 20, 25, 30 μmol/L in human sweat or urine samples. These results indicate that the CDs@GC nanosensor based platform is effective and reliable for the detection of DA in complicated samples and could further confirm the feasibility of this EED theory.

In summary, we developed an innovative "Enrichment-enhanced Detection" strategy for the enhanced detection of dopamine using a CDs@GC nanosensor. The GC of the nanocomplex can effectively increase the local concentration of the analyte to significantly improve the sensitivity and selectivity of the sensing system. The LOD of the nanosensor was determined as 3.7 nmol/L, demonstrating 12-fold enhancement in the sensitivity compared to bare CDs probe with similar fluorescent profile. Subsequently, we applied this strategy to the design of a high-performance portable platform for the visual detection of dopamine (DA) to further explore the feasibility of EED strategy in real case. The success of this CDs@GC-DA detecting system exhibited the potential of this novel strategy as a universal optimizing pathway for the development of high-performance probes.

Declaration of competing interest

The authors declare that they have no known competing financial interests or personal relationships that could have appeared to influence the work reported in this paper.

CRediT authorship contribution statement

Xilin Bai: Conceptualization, Data curation, Formal analysis, Funding acquisition, Investigation, Methodology, Project administration, Validation, Visualization, Writing – original draft, Writing – review & editing. **Wei Deng:** Investigation. **Jingjuan Wang:** Writing – original draft. **Ming Zhou:** Supervision, Writing – original draft, Writing – review & editing.

Acknowledgments

The author gratefully acknowledges the financial support from the National Natural Science Foundation of China (No. 21904007), the Fundamental Research Funds for the Central Universities (China, No. 2412022QD008), the Jilin Provincial Department of Education (China), the Key Laboratory of Nanobiosensing and Nanobioanalysis at Universities of Jilin Province (China), and

the Analysis and Testing Center of Northeast Normal University (China).

Supplementary materials

Supplementary material associated with this article can be found, in the online version, at doi:10.1016/j.cclet.2024.109959.

References

[1] R. Gui, H. Jin, X. Bu, et al., Coordin. Chem. Rev. 383 (2019) 82–103.
[2] X. Chai, H.H. Han, A.C. Sedgwick, et al., J. Am. Chem. Soc. 142 (2020) 18005–18013.
[3] L. Gao, W. Wang, X. Wang, et al., Chem. Soc. Rev. 50 (2021) 1219–1250.
[4] J. Chen, H.D. Qiu, Chin J. Chromatogr. 41 (2023) 825–834.
[5] D. Wang, H. Li, H. Qiu, et al., J. Anal. Test. 7 (2023) 8–15.
[6] J. Chen, N. Yuan, D. Jiang, et al., Chin. Chem. Lett. 32 (2021) 3398–3401.
[7] L. Basabe-Desmonts, D.N. Reinhoudt, M. Crego-Calama, Chem. Soc. Rev. 36 (2007) 993–1017.
[8] M. Schäferling, Angew. Chem. Int. Ed. 51 (2012) 3532–3554.
[9] S.A. Nsibande, P.B.C. Forbes, Anal. Chim. Acta. 945 (2016) 9–22.
[10] S. Shen, W. Xu, J. Lu, et al., Chin. Chem. Lett. 35 (2024) 108360.
[11] X. Bai, S. Xu, L. Wang, Anal. Chem. 90 (2018) 3270–3275.
[12] C. Missale, S.R. Nash, S.W. Robinson, et al., Physiol. Rev. 78 (1998) 189–225.
[13] J.D. Berke, Nat. Neurosci. 21 (2018) 787–793.
[14] K.H. Wang, A. Penmatsa, E. Gouaux, Nature 521 (2015) 322–327.
[15] R. Franco, I. Reyes-Resina, G. Navarro, Biomedicines 9 (2021) 109.
[16] M.O. Klein, D.S. Battagello, A.R. Cardoso, et al., Cell. Mol. Neurobiol. 39 (2019) 31–59.
[17] E. Monzani, S. Nicolis, S. Dell'Acqua, et al., Angew. Chem. Int. Ed. 58 (2019) 6512–6527.
[18] A. Mohebi, J.R. Pettibone, A.A. Hamid, et al., Nature 570 (2019) 65–70.
[19] W. He, R. Gui, H. Jin, et al., Talanta 178 (2018) 109–115.
[20] J. Wu, W. Liu, J. Ge, et al., Chem. Soc. Rev. 40 (2011) 3483–3495.
[21] M. Xie, J. Chen, Y. Wang, et al., Chin. Chem. Lett. 35 (2024) 108575.
[22] L. Yu, L. Feng, L. Xiong, et al., Nanoscale 13 (2021) 11188–11196.
[23] X. Qu, C. Gao, L. Fu, et al., ACS Appl. Mater. Interfaces 15 (2023) 18608–18619.
[24] R. Qiang, H. Huang, J. Chen, et al., ACS Appl. Mater. Interfaces 15 (2023) 38653–38664.
[25] J. He, J. Chen, H.D. Qiu, Prog. Chem. 35 (2023) 655–682.
[26] M. Louleb, L. Latrous, Á. Ríos, et al., ACS Appl. Nano Mater. 3 (2020) 8004–8011.
[27] Y.S. He, C.G. Pan, H.X. Cao, et al., Sensor. Actuat. B: Chem. 265 (2018) 371–377.
[28] Y. Ma, A.Y. Chen, X.F. Xie, et al., Talanta 196 (2019) 563–571.
[29] X. Ren, J. Ge, X. Meng, et al., Sci. Bull. 61 (2016) 1615–1623.
[30] D. Diaz-Diestra, B. Thapa, J. Beltran-Huarac, et al., Biosens. Bioelectron. 87 (2017) 693–700.
[31] G.L. Wang, F. Yuan, T. Gu, et al., Anal. Chem. 90 (2018) 1492–1497.
[32] Z. Ma, Y. Xu, P. Li, et al., Anal. Chem. 93 (2021) 3586–3593.
[33] X. Guo, J. Wu, L. Xia, et al., Sci. China Chem. 63 (2020) 1012–1018.
[34] S. Chu, H. Wang, X. Ling, et al., ACS Appl. Mater. Interfaces 12 (2020) 12962–12971.
[35] M. Xiao, Z. Liu, N. Xu, et al., ACS Sens. 5 (2020) 870–878.
[36] Y. Ye, T. Wu, X. Jiang, et al., ACS Appl. Mater. Interfaces 12 (2020) 14552–14562.